



Multilayer Graphene-Coated Silicon Carbide Nanowire Formation Under Defocused Laser Irradiation

Kanon Minami¹ · Kyosuke Kobinata² · Jiwang Yan¹

Received: 11 March 2023 / Revised: 20 May 2023 / Accepted: 21 May 2023
© The Author(s) 2023

Abstract

Graphene-coated silicon carbide (SiC@C) core-shell nanostructures have attracted attention in the fields of energy storage and nanoelectronics. In this study, multilayer graphene-coated silicon carbide (SiC) nanowires were obtained through the laser irradiation of a mixture target of graphite powder and silicon (Si) grinding sludge discharged from Si wafer manufacturing. Laser irradiation was performed using an ytterbium (Yb) fiber pulsed laser with a pulse width of 10 ms and a wavelength of 1070 nm with various defocus distances. The effect of laser defocusing on the morphology of the generated nanostructures was investigated. Results showed that nanowires were produced under the defocused conditions, and nanoparticles were observed at the on-focus position. The products obtained under all defocused conditions showed a core-shell structure, and the SiC nanowires were covered by graphene layers. The aspect ratio of the nanowires increased with the defocus distance. Observation of the laser-induced plume using a high-speed camera showed that when the laser was defocused, the plume propagation speed slowed down, and the shape of the plume changed to a swirling vortex. The nanowire formation was closely related to the propagation speed and shape variation of the plume. This successful production of SiC@C core-shell nanowires from Si waste opens up the possibility of the sustainable development of new materials for energy storage and nanoelectronics.

Highlights

- The shape of the produced nanostructures is changed from nanoparticles to nanowires by defocusing the laser beam.
- The SiC nanowires have core-shell structures and are covered by multilayer graphene.
- Under defocused conditions, the plume swirls as a vortex moving at a low speed, thus promoting nanowire growth.

Keywords Nanomaterial · Laser irradiation · Silicon carbide · Nanowire · Silicon sludge · Core-shell structure · Multilayer graphene

1 Introduction

Semiconductor manufacturing is an essential part of electronic devices and photovoltaic industry. In this process, a huge amount of silicon (Si) sludge is generated in powder form during the slicing and grinding of Si wafers and

disposed of as industrial waste [1–3]. This practice constitutes a tremendous loss of material resources and energy and a potential threat to the environment. Thus, the recycling destinations of Si sludge are being considered to realize closed-loop sustainable manufacturing [4, 5].

Nanosized materials, such as the nanoparticles [6] and nanowires [7] of Si and silicon carbide (SiC) [8], have excellent cyclability and theoretical capacity and are expected to be applied as one of the most important anode alternatives for lithium-ion batteries. For other applications, 3C-SiC nanowires have excellent mechanical properties, field emission properties [9, 10], and biocompatibility [11, 12]. They have demonstrated remarkable dielectric and conductive properties [13] when coated with carbon (C). Coating

✉ Jiwang Yan
yan@mech.keio.ac.jp

¹ Department of Mechanical Engineering, Faculty of Science and Technology, Keio University, Hiyoshi 3-14-1, Kohoku, Yokohama 223-8522, Japan

² DISCO Corporation, 13-11 Omori-Kita 2-Chome, Ota-Ku, Tokyo 143-8580, Japan

SiC nanowires with amorphous carbon improve their field emission properties [14]. SiC nanowires and C-coated SiC nanowires, namely, SiC@C core-shell nanowires, have been proposed as anodes in lithium-ion batteries and as field emission displays [14] and nanoelectrodes [15, 16] that can be used inside living cells. They are expected to be applied in fields such as nanoelectronics with high durability and stability, even in harsh environments. On these backgrounds, tremendous industrial and social merits can be expected if Si sludge can be transformed into Si/SiC-based nanomaterials.

Previous studies have reported the generation of Si nanostructures such as Si nanoparticles [17, 18] and Si nanofibers [19] by irradiating Si slicing/grinding sludges with nanosecond and millisecond pulsed lasers. Si nanoparticles are also produced by femtosecond pulsed laser irradiation [20] and laser irradiation in liquid [21]. These methods generate nanostructures through the cooling and agglomeration of plumes generated during laser irradiation. By adding graphite powder to Si grinding sludge and irradiating the mixture with a millisecond pulsed laser, Minami et al. succeeded in producing graphene-coated 3C-SiC nanoparticles with a core-shell structure [22]. However, the possibility of producing Si/C composite nanowires with graphene coatings using Si sludge has never been reported.

In laser irradiation, the shape and velocity of the plume can be changed by varying the laser irradiation conditions, such as laser beam defocusing. These changes would affect the melting, evaporating, and cooling rates and the movement patterns of materials in the plume, which in turn lead to various mechanisms for nanomaterial growth and chemical reactions. The morphology of the resulting nanostructures may change from nanoparticles to nanowires, nanofibers, or other high aspect ratio nano-objects if the plume duration time is sufficiently long for their epitaxial growth.

This study aimed to produce Si/C composite nanowires with multilayer graphene coatings from Si grinding sludge. Si sludge generally contains impurities, such as SiC or diamond abrasive grains, making it difficult to be reused. Here, Si sludge was transformed once inside a plasma plume where a chemical reaction occurs. In the plasma plume, the abrasive grains also transform into Si and C species so that the existing SiC and diamond abrasive grains do not become impurities in the final product. The use of Si sludge as a precursor is of substantial importance from the perspective of waste reuse. The application of this composite is important because it is compatible with Si sludge and has the potential to transform waste into batteries and electronic materials. However, generating SiC nanowires from the mixed composite is technically more difficult compared with the SiC substrates previously reported [23]. Therefore, a series of experiments was conducted by laser defocusing, i.e., gradually changing the distance between the target and focal point, to explore the possible conditions in which nanowires can be

produced by laser irradiation. The generated nanostructures were collected and characterized in detail. The effects of defocusing-induced changes in energy density and laser spot size on the morphology of the products were investigated. The plume volume change was also determined by measuring the target after irradiation and examining the amount of material scattered. The expectation is that Si/C composite nanowires with multilayer graphene coatings could be generated via laser defocusing. This work provides a potential method to synthesize anode materials for manufacturing advanced lithium-ion batteries and other electronic devices.

2 Experimental Methods

2.1 Target Preparation

The target generation process is shown in Fig. 1a. The Si sludge used in the experiment was obtained by grinding Si wafers, and its average grain size was 3.9 μm . The Si sludge was mixed with graphite powders with an average grain size of 50 μm (Kojundo Chemical Laboratory Co., Ltd., Japan) at a ratio of 1:2 (wt.%) and mill ground for 3 h using a pot mill. After pot milling, the Si particle size decreased to $\sim 1 \mu\text{m}$, and the C particle size was also slightly reduced, as shown in the scanning electron microscope (SEM) image in Fig. 1b. The mixed powder was placed in a tablet molding machine, and a 40 kN load was applied for 1 min at room temperature to produce a cylindrical Si/C mixed target with a diameter of 1.0 cm.

2.2 Laser Irradiation

Figure 2a shows a top view of the experimental setup for laser irradiation. In a chamber filled with argon gas at a pressure of 0.1 MPa, an ytterbium (Yb) single-mode CW laser (YLR-500-AC, IPG Photonics Co., USA) with a wavelength of 1070 nm, an output of 390 W, and Gaussian energy distribution was used to generate pulse waves with a pulse width of 10 ms. Each target was irradiated with a single shot in the experiment. The laser beam focused on the target surface using a condensing lens with a focal length of 200 mm. A glass substrate was placed 5 mm below the laser beam to collect the products generated during laser irradiation. As shown in Fig. 2b, the target was gradually relocated away from the focal point to four different defocused positions (15, 20, 24, and 28 mm) by horizontally moving the target holder. The changes in laser beam profile and spot size of the fiber laser system are shown in Fig. 3a. The light emitted from the fiber was collimated and then focused by a set of lenses.

The resulting beam waist ω_0 can be calculated from the beam diameter D of the collimated light, the beam quality

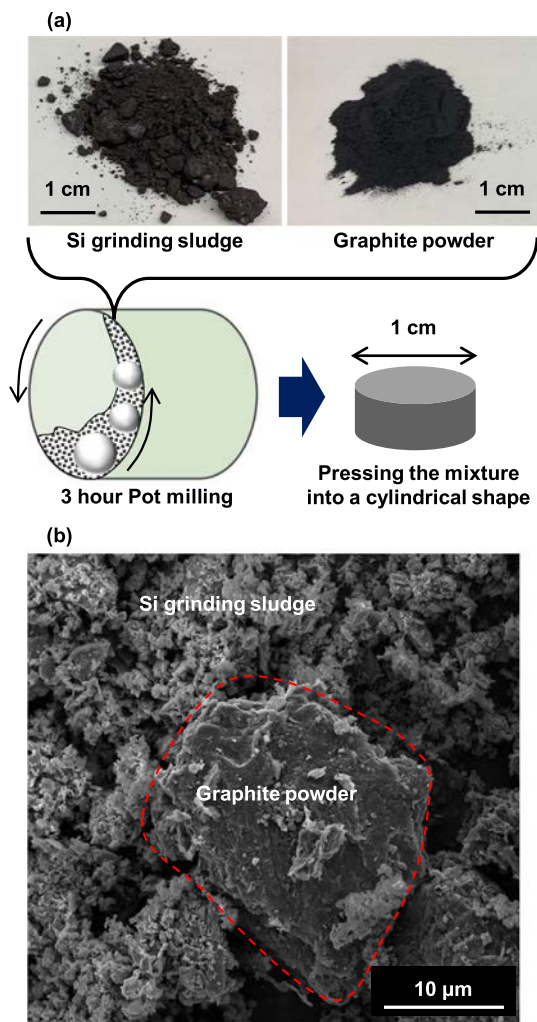


Fig. 1 a Silicon (Si)/carbon (C) mixed target preparation process; b the scanning electron microscope (SEM) image of Si sludge and graphite powder after milling

factor M^2 , the focal length f of the lens, and the wavelength λ of the laser as expressed by Eq. (1).

$$\omega_0 = \frac{2M^2 \lambda f}{\pi D} \tag{1}$$

In this study, the beam quality factor was $M^2 = 1.05$, and the measured laser beam diameter was $D = 12.6$ mm. Thus, the theoretical beam waist ω_0 was 11.4 μm . The expansion angle θ of the laser beam shown in Fig. 3b can be obtained using Eq. (2).

$$\theta = \frac{M^2 \lambda}{\pi \omega_0} \tag{2}$$

Using the value of θ , the spot radius ω_z can be obtained by Eq. (3) when the defocus distance is L .

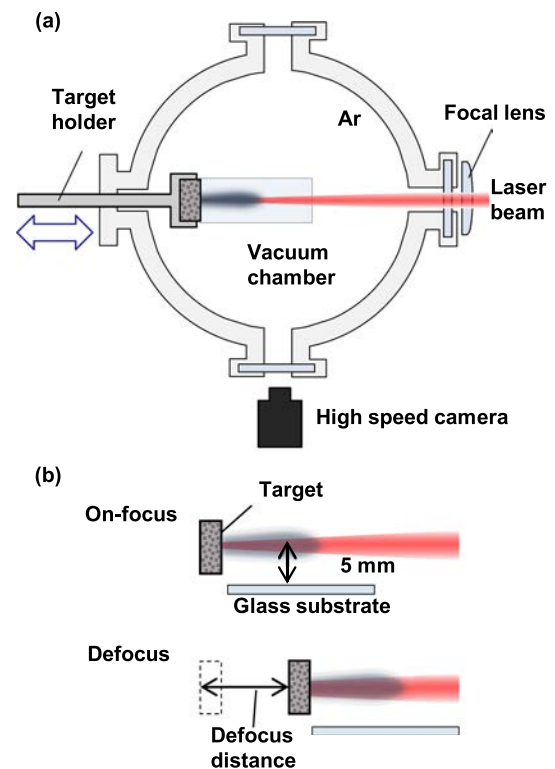


Fig. 2 Experimental setup for laser irradiation: a top view and b side view

$$\omega_z \approx L\theta \tag{3}$$

When the laser power is P_0 , the power density can be obtained from Eq. (4):

$$P(r) = \frac{2P_0}{\pi \omega_z^2} \exp\left(-\frac{2r^2}{\omega_z^2}\right) \tag{4}$$

The calculated power density varies with defocus distance, as shown in Fig. 3c and d.

2.3 Material Characterization

The morphology of the products deposited on the glass substrate was observed using field emission scanning electron microscopy (FE-SEM, Inspect F50, FEI Company, USA) and transmission electron microscopy (TEM, Tecnai G2, FEI Company, USA). The deposits were collected in five single-shot irradiations at a defocus length from 15 to 28 mm to obtain adequate products for TEM observation. As shown in the TEM images, 25 arbitrary nanowires were extracted for the 15 mm defocused condition and 50 arbitrary nanowires for the 20, 24, and 28 mm defocused conditions. The diameter and length of the nanowires were measured to investigate the mechanism

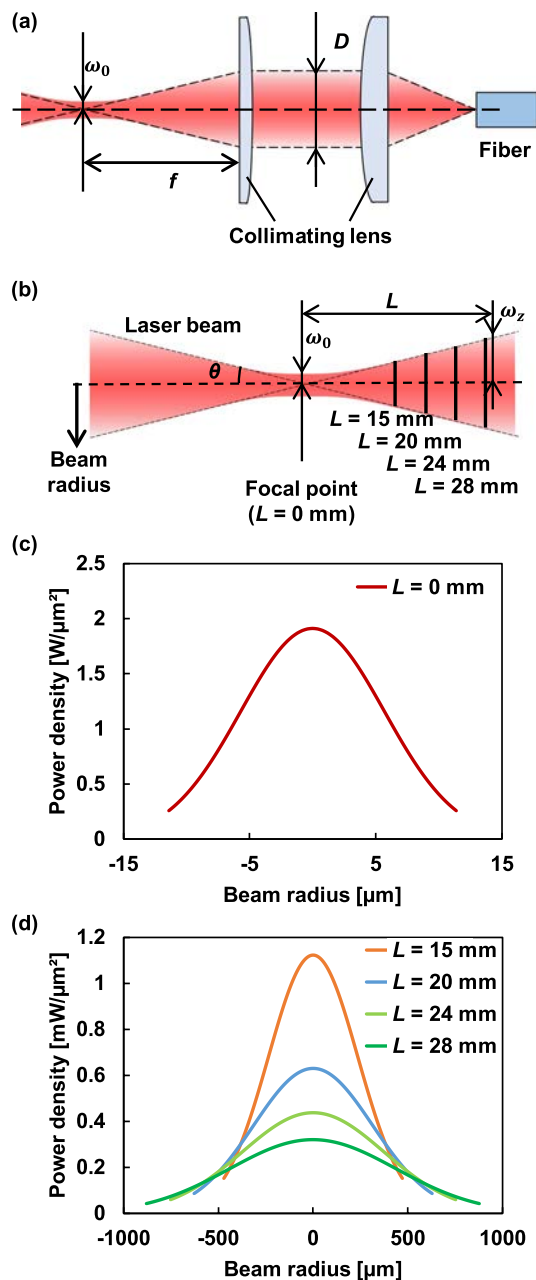


Fig. 3 **a** Beam waist of a fiber laser; **b** change of beam radius with defocus distance; power density distributions under **c** on-focus condition and **d** defocused conditions

of nanowire growth. The composition of the nanoparticles was also evaluated from the selected area electron diffraction pattern by TEM.

The target was observed and measured using a laser microscope (VK-X1000, KEYENCE Co., Japan) to confirm the amount of material removed from the target after single-shot irradiation. The volume of the crater formed on the target surface by laser irradiation was estimated from the cross-sectional profile of the crater.

2.4 Plume Observation

The laser-induced plume was photographed using a high-speed camera FASTCAM Mini AX50 (Photron Ltd., Japan). Two types of shooting were carried out: general shooting mode and shooting with the Schlieren method. The general shooting mode is suitable for observation from the start of laser irradiation to the end of laser irradiation; however, the subsequent phenomenon is not visible when the light emitted by the laser irradiation ends. The Schlieren method allows observation of the plume after laser irradiation and is effective for understanding the plume [24]. A schematic of the light path in the Schlieren method plume observation is shown in Fig. S1 in the supplementary information. The plume to be observed was set in the collimated light produced by a point light source and two collimating lenses. The light was disrupted and refracted by the plume, allowing the density gradient of the plume to be visualized. In this study, a light source with a diameter of 4.3 mm was covered with a pinhole with a diameter of 1.5 mm. The illuminance at a distance of 10 cm from the light source was 3000 lx without the pinhole and 200 lx with the pinhole. A pinhole with a diameter of 1.5 mm was also placed in front of the high-speed camera as a knife edge. The plume can be observed after the irradiation has finished because a point light source is used. Changes in the shape and propagation rate of the plume can be visualized by observing the plumes produced by these two methods under focus and defocus conditions. In the general shooting mode, images were taken at a frame rate of 4000 fps and a shutter speed of $1/950,000$ s. In shooting using the Schlieren method, images were taken at a frame rate of 10,000 fps and a shutter speed of $1/100,000$ s. The distance propagated by the plume was measured from the Schlieren method shooting in 0.1 ms increments during the first 2 ms of irradiation and in 0.5 ms increments throughout the remaining irradiation, and the plume propagation speed was determined for each condition.

3 Results and Discussion

3.1 Defocus-Induced Nanoparticle/Nanowire Transition

Figure 4 shows the SEM images of the deposits under various conditions. Under the on-focus condition (Fig. 4a, b), almost all the products were nanoparticles. When the laser was defocused, nanowires were generated along with nanoparticles, and the number of nanowires increased with the defocus distance (Fig. 4c–f). The products included nanostructures that are too short to be called nanowires. However, in this study, we referred to this kind of nanostructures as nanowires to distinguish them from nanoparticles.

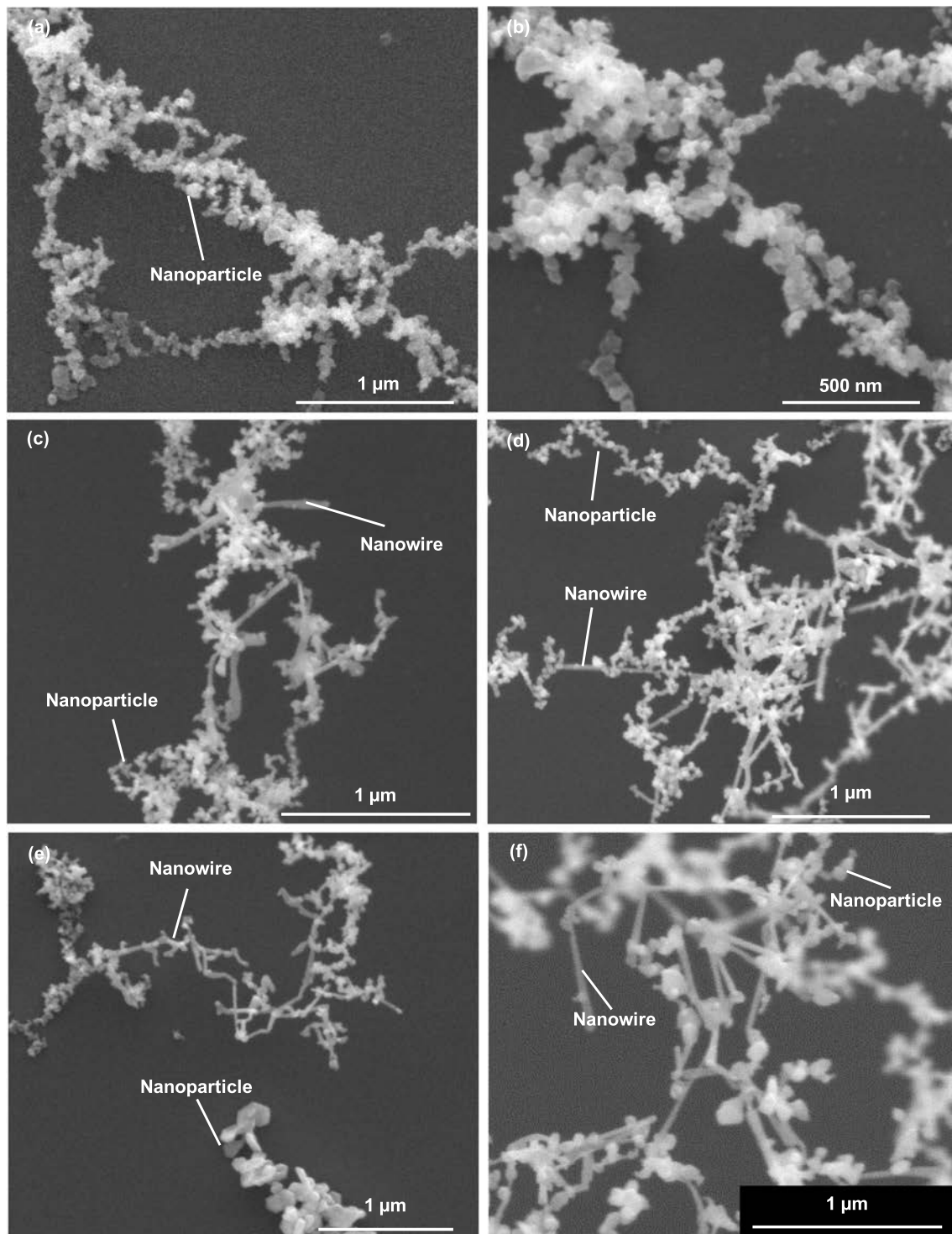


Fig. 4 SEM images of nanostructures under defocused distances of **a**, **b** 0, **c** 15, **d** 20, **e** 24, and **f** 28 mm

Figure 5 shows a TEM image of the nanowires at low magnification. Three types of nanowires were identified: nanowires with spherical or polygonal caps at the tip and nanowires without caps. Figure 6 shows a graph of nanowire diameters and lengths for each of the conditions under which

nanowires were produced. The diameter of the nanowires (Fig. 6a) did not show a clear correlation with the defocus distance; but their length (Fig. 6b) showed a tendency to increase with the defocus distance. The length of the nanowires did not change much between the defocus distances of

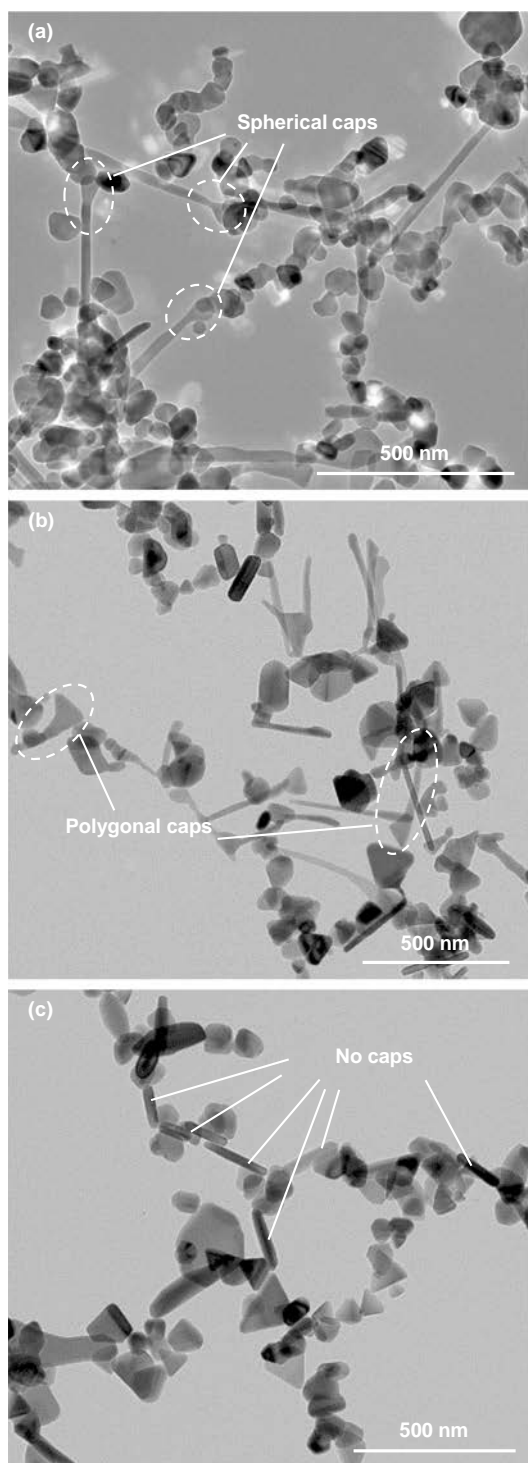


Fig. 5 The transmission electron microscopy (TEM) images of nanowires having **a** spherical caps, **b** polygonal caps, and **c** no caps under 28 mm defocused distance

20 and 24 mm. A possible reason is the nonuniformity of the target. The target used in this study is composed of powders of two different elements, each with a different grain size. After mixing, the material might have exhibited a

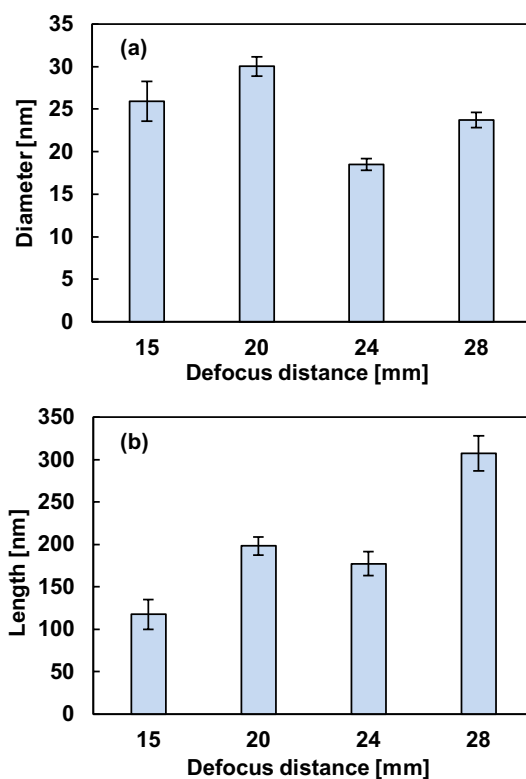


Fig. 6 Change in nanowire: **a** diameters and **b** lengths with defocusing

nonuniform distribution on the target surface, resulting in small differences in the length of the nanowires produced. The frequencies of the nanowire aspect ratios (length/diameter) are shown in Fig. 7. The highest number of nanowires with an aspect ratio of < 5 were observed at a defocus distance of 15 mm, the highest number of nanowires with an aspect ratio between 5 and 10 were observed at defocus distances of 20 and 24 mm, and several nanowires with an aspect ratio exceeding 20 were observed at a defocus distance of 28 mm. The longer the defocus distance, the higher the aspect ratio of the nanowires produced.

3.2 Material Composition/Structure Analysis

High-magnification TEM images of the nanoparticles are shown in Fig. 8. At the on-focus position, almost all nanoparticles were surrounded by graphene layers. This finding is consistent with the results of a previous study on the formation of core-shell particles [22]. The deposition of graphene layers under defocused conditions was also confirmed. Multilayer graphene deposition was also observed in the nanowires at high magnification, as shown in Fig. 9. On the basis of these results, a core-shell structure with graphene layers deposited on the nanoparticles and nanowires was generated under all conditions. The

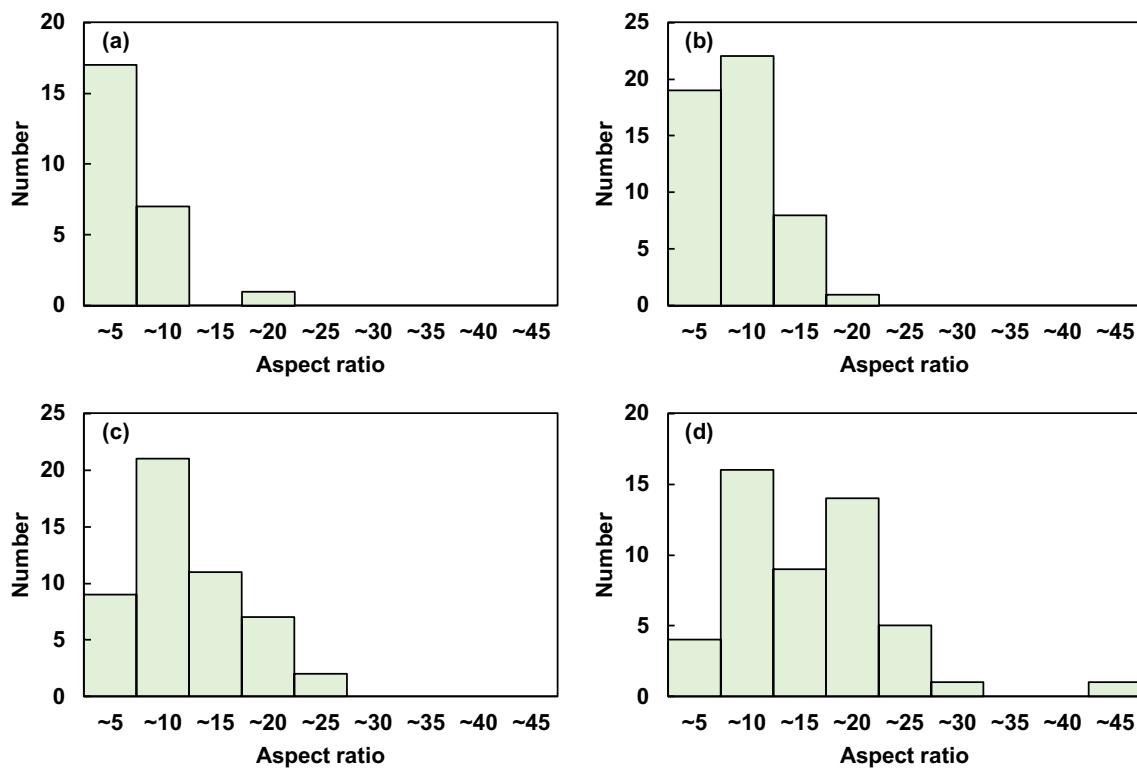


Fig. 7 Frequencies figure of the nanowire aspect ratios under various defocused distances: **a** 15, **b** 20, **c** 24, and **d** 28 mm

energy-dispersive X-ray spectroscopy (EDX) mapping images shown in Fig. 10 confirm that the nanowires were mainly composed of Si and C elements. Nanowires with caps (Fig. 10a, b) also contained Si and C elements in their wire and cap parts.

The electron diffraction patterns (Fig. 11) under all conditions were evaluated by TEM. Given that 3C-SiC and 6H-SiC have similar crystal structures, they have many common electron diffraction patterns [25–27]. However, the pattern for 6H-SiC {101} and {103} did not overlap with that of 3C-SiC [26, 27]. These patterns were used as an indicator to confirm the presence of 6H-SiC. 6H-SiC {101} was confirmed to be present under 20 (Fig. 11c), 24 (Fig. 11d, e), and 28 mm (Fig. 11f) defocused conditions, but the number of bright spots was small in all conditions. No pattern indicating {103} was observed in any of the conditions; the patterns common to 3C-SiC were all strongly bright, suggesting that 3C-SiC and 6H-SiC are both present, but the content of 3C-SiC may be higher than that of 6H-SiC.

In some TEM images, bright spots indicating C [28] (Fig. 11c, e) and Si [29] (Fig. 11e) were observed. The graphene layers being thinner than the nanoparticles and nanowires might have prevented the appearance of bright spots. In conclusion, the main product was multilayer graphene deposited 3C-SiC nanostructures with low contents of 6H-SiC and Si.

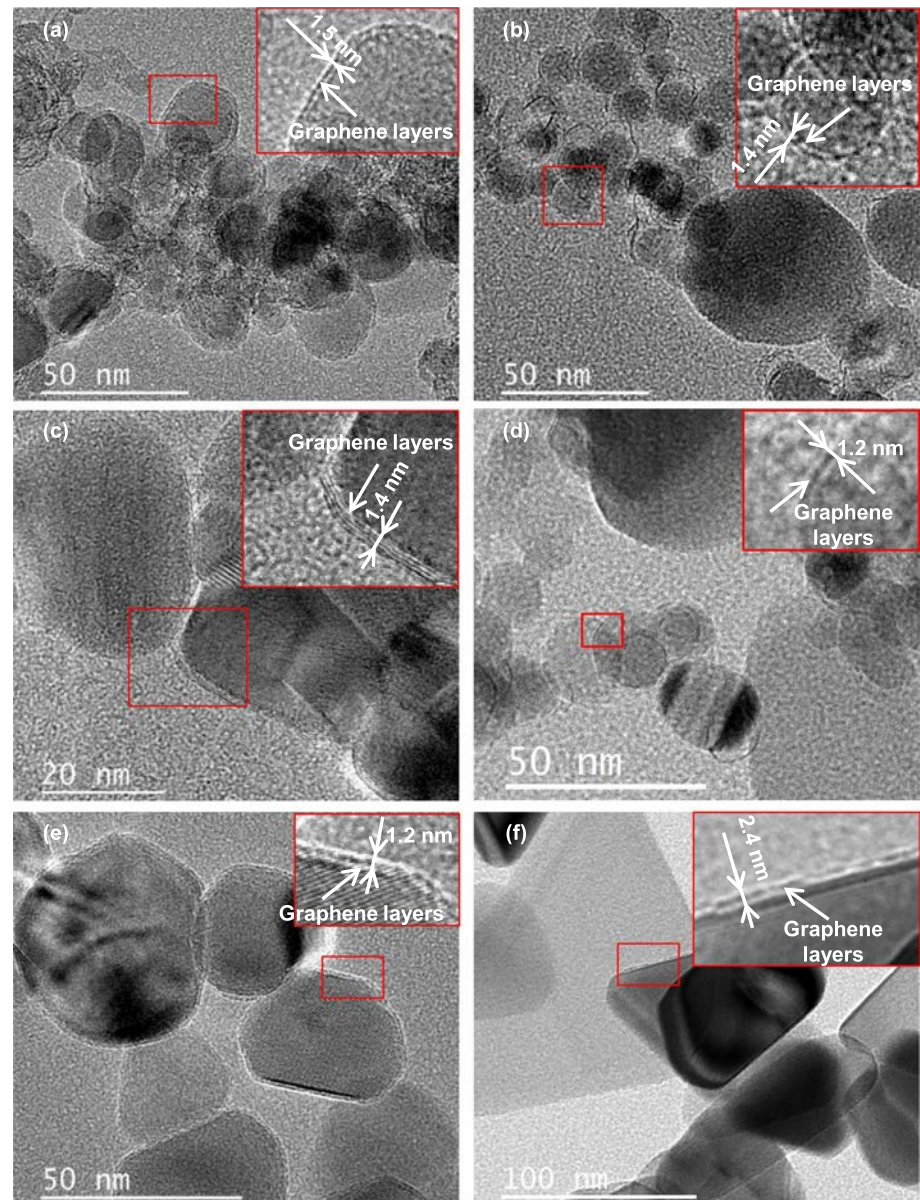
3.3 Material Volume Analysis

The targets after single-pulse irradiation were measured using a laser microscope. The cross-sectional profile of the holes created by these irradiations is shown in Fig. 12, and the relationship between the volume of the removed portion and defocusing is displayed in Fig. 13. The hole diameter increased with defocusing distance, but the hole depth became shallow. According to the 3D morphology measurement, the amount of removed material reached a maximum at a defocus of 15 mm and decreased with a further increase in defocused distance. In laser irradiation, the hole in the irradiated target becomes deeper and smaller in diameter as the energy level increases [30] because the amount of energy per unit area decreases with defocusing, as shown in Fig. 3c, d. This result showed that the generated plume volume increased due to the increase in energy per unit area. Photographs showing the holes caused by these irradiations are included in Fig. S2 in the supplementary information.

3.4 Plume Shape Comparison

Figure 14 shows images of the plume from the start of laser irradiation to 4.5 ms after the irradiation taken in the general shooting mode. The plume was generated immediately from the target irradiated at the focus position. When the

Fig. 8 TEM images of graphene layers on the nanoparticles under defocused distance of **a** 0, **b** 15, **c**, **d** 20, **e** 24, and **f** 28 mm



target was moved in the defocus direction, additional time was required between irradiation and plume generation. This phenomenon occurred because the power density decreased due to defocusing, and the target seemed to require a few milliseconds to be sufficiently heated. Figure 15 shows images of the plume from the start of laser irradiation to the end of laser irradiation taken in the general shooting mode. In Fig. 15a–c, the plume extended beyond the screen. However, in Fig. 15d, e, the plume was contained within the area photographed, indicating that the length of the plume in the direction of propagation shortened as the laser defocused. Research using nanosecond pulsed lasers showed that the higher the laser energy, the larger the plume extends in the direction of the laser source [31]. The same phenomenon can also be observed with millisecond pulses.

In addition to its length, the shape of the plume differs under focused and defocused conditions. An enlarged view of the plume in the focus condition and the plume in the 28 mm defocus distance is shown in Fig. 16. In the focused state, the plume moved in one direction without swirling. In the defocused state, the plume propagated in a swirling manner. For clarifying the behavior of the plume, the Schlieren image of the plume after the irradiation is shown in Fig. S3 in the supplementary information. At 24 and 28 mm defocus distances, the plume propagated slowly even after the irradiation was finished. The position of the plume progression was examined at 0.1 ms intervals by feeding the Schlieren image frame by frame, and the results are shown in Fig. 17. The approximate curves of the plot showed that the plume propagation speed for each

Fig. 9 TEM images of graphene layers on the nanowires under defocused distance of **a** 15, **b** 20, **c** 24, and **d** 28 mm

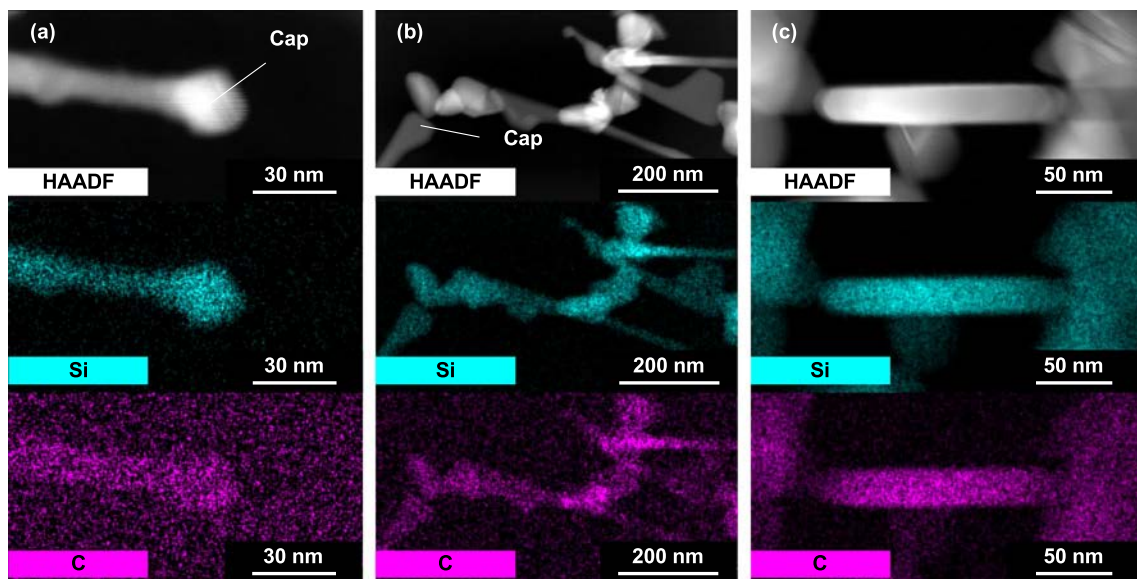
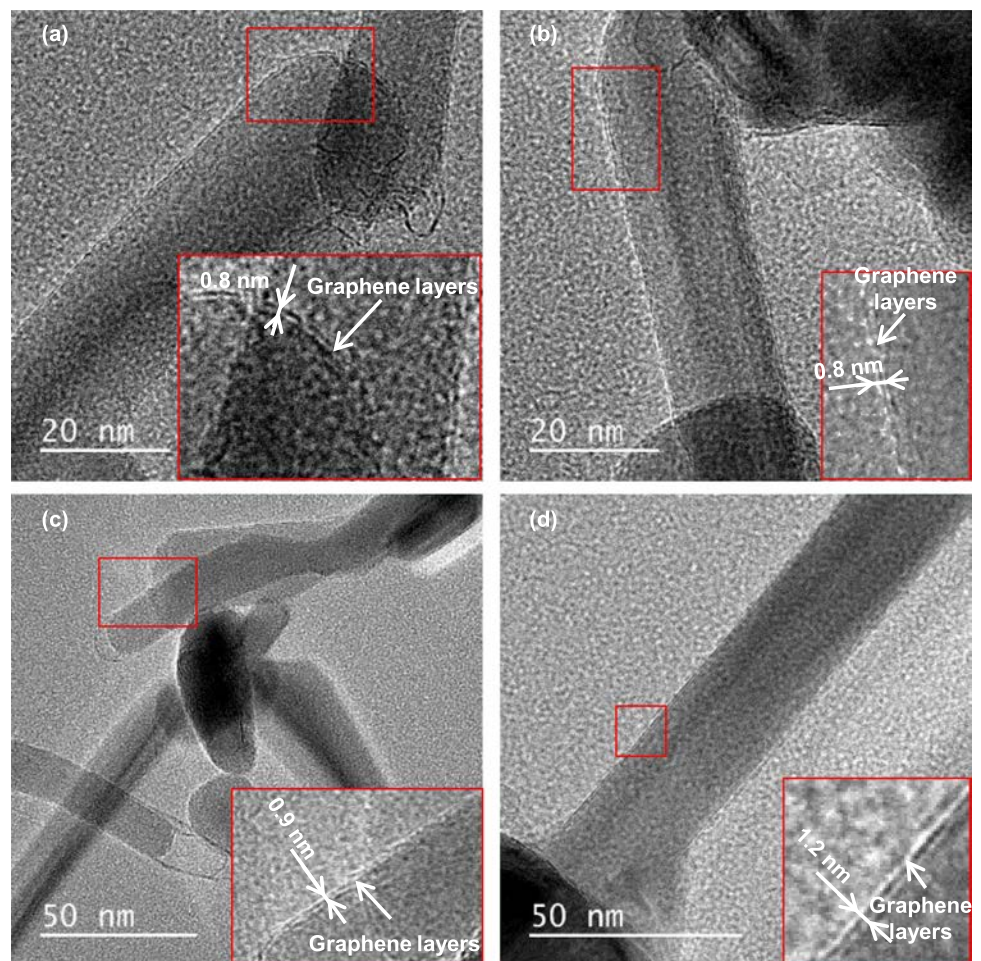
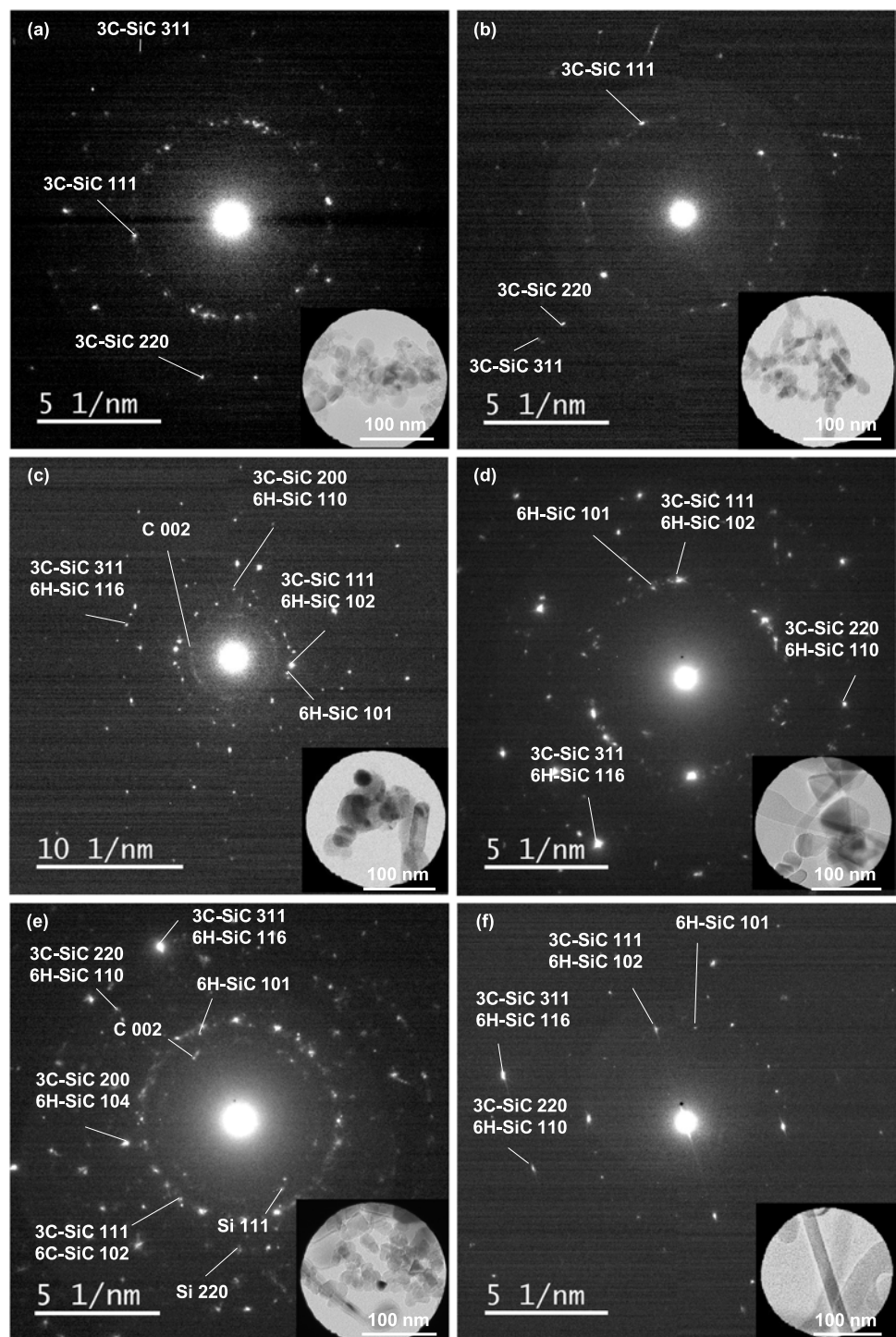


Fig. 10 The energy-dispersive X-ray spectroscopy (EDX) mapping analysis of nanowires which have **a**, **b** with caps and **c** no caps generated under a defocused distance of 28 mm

Fig. 11 The selected area electron diffraction patterns from TEM images under defocused distance of **a** 0, **b** 15, **c** 20, **d**, **e** 24, and **f** 28 mm



condition was 12.85 mm/ms for the on-focus condition, 6.85 mm/ms for the 15 mm defocused condition, 3.14 mm/ms for the 20 mm defocused condition, 1.34 mm/ms for the 24 mm defocused condition, and 0.68 mm/ms in the 28 mm defocused condition. The growth rate of the plume was relatively slow in the defocused state.

3.5 Hypothesis of Nanowire Growth Mechanism

SiC@C core-shell nanoparticles and nanowires were obtained as final products, and their 3D microstructures are shown schematically in Fig. 18. SiC cores have excellent battery storage and electrolytic discharge properties, and graphene shells provide dielectric and conductive properties [8, 13]. In this section, the formation mechanism for

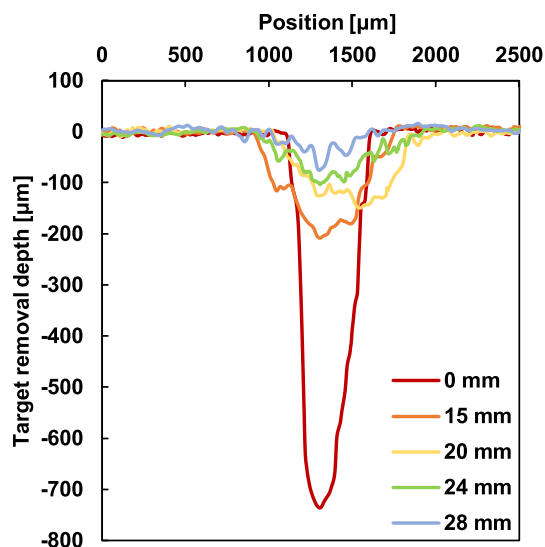


Fig. 12 Cross-sectional profile of the holes created by laser irradiation

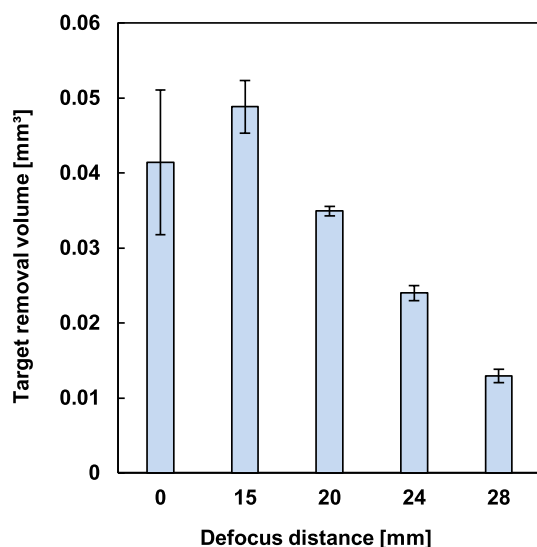


Fig. 13 Change in the volume of the removed portion with defocusing

these products was discussed. If the mechanism of composite material formation by laser can be clarified, then it could be applied to the formation of other composite materials. Composite materials, as typified by core-shell structures, are expected to be applied in a wide range of fields, such as power electronics [32, 33].

Laser irradiation of a solid target generates a plume [24]. The plume mainly consists of plasma and sublimated vapor [25], and nanodroplets are mixed in when millisecond pulses are irradiated [26, 27]. The plume is cooled down by collision with the ambient gas, resulting in nanoparticles or

nanowires. The temperature and substance distributions inside the plume are complex, and the chemical reactions have a random nature. For example, while the inner part of the plume is under high temperature, the outer part of the plume could come into contact with the ambient gas and is prone to rapid cooling. Rapid cooling of the plume promotes nanoparticle production. Methods of nanoparticle production include femtosecond pulsed laser ablation [20] and nanosecond pulsed laser ablation [21] in water. Rapid cooling is an important factor in nanoparticle production; for example, the use of a short pulse width generates nanoparticles because of rapid cooling due to the low plume volume, and rapid cooling in water results in nanoparticles. Under the on-focus condition with millisecond pulsed lasers in this study, rapid cooling was facilitated by fast plume diffusion. The characteristic feature of a millisecond laser plume is that melting and evaporation occur intensely, so the plume volume is higher than that of nanosecond and femtosecond pulsed lasers, and the plume contains abundant droplets. Thus, the plume contains a mixture of droplets and gases, and the produced nanowires have different shapes depending on which state they originated from. Therefore, many types of products with different shapes and compositions are produced simultaneously, such as amorphous and crystalline nanoparticles and tipped and untipped nanowires. Some factors affect the morphology and the formation mechanism of the nanostructures produced by laser irradiation. Figure 19 shows a schematic of the possible nanowire formation mechanisms. The mechanisms of nanowire formation in this study can be classified into two categories: vapor-liquid-solid (VLS) growth (Fig. 19a) and vapor-solid (VS) growth (Fig. 19b).

In VLS growth, a metal catalyst is usually used to form supersaturated droplets by supplying raw gas to the metal droplets from which nanowires are grown [34–36]. In this study, Si droplets took this position, although no metal catalyst was used. Si has droplet and gaseous plumes, and C has only a gaseous plume [22]. The formation of self-catalytic Si nanowires by Si droplets [37] and SiC nanoparticles through the reaction between Si droplets and carbon species has already been reported [38]. As shown in Fig. 19a, the diffusion of a large number of carbon species into the Si droplet produces Si-C particles, which have instability due to further continuous feeding and consequently form nanowires [39]. The nanowires produced by this mechanism are characterized by a cap at the tip, a remnant of the droplet, as shown in Fig. 5a, b. The spherical cap (Fig. 5a) is amorphous SiC, and the polygonal cap (Fig. 5b) is a shape indicative of crystalline SiC [39].

By contrast, nanowires synthesized by the VS method [10, 40, 41] are noncatalytically produced and characterized by the absence of a cap at the tip [42]. In this study, oxygen removal was not carried out for the starting materials,

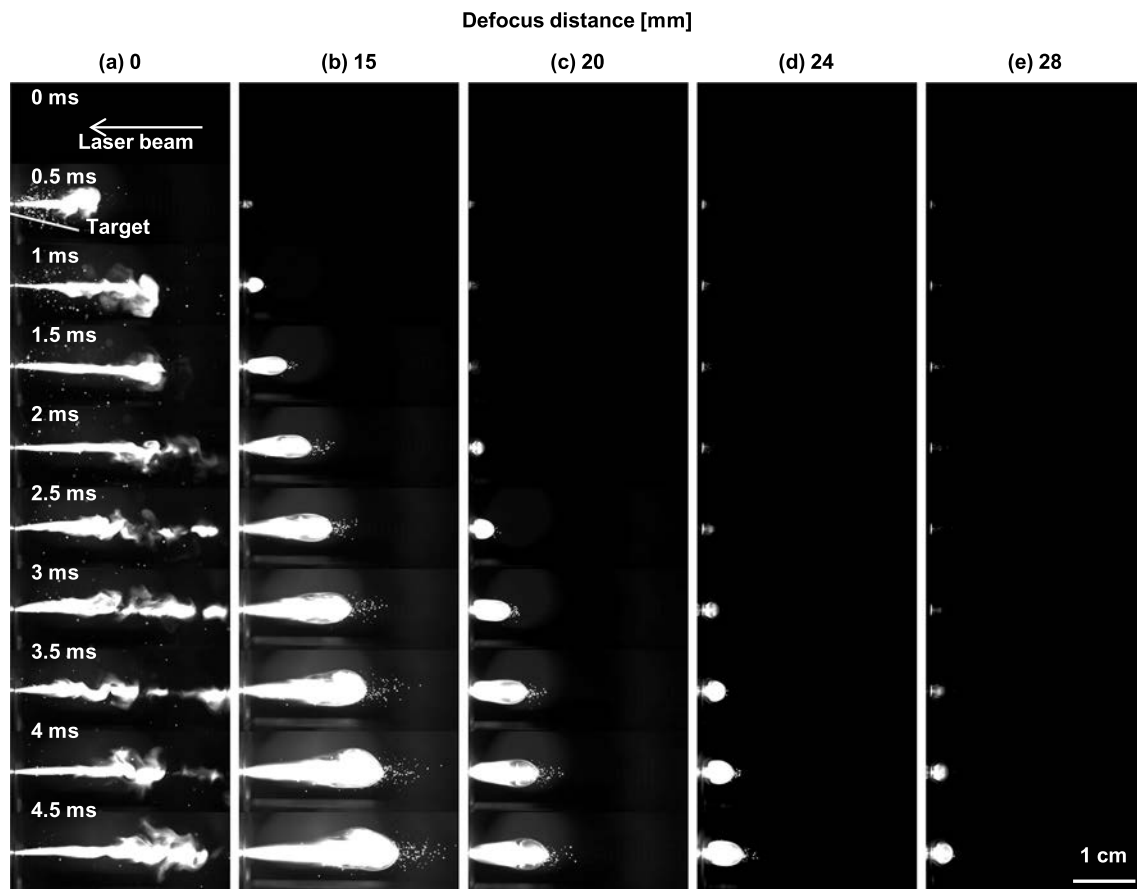
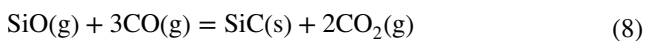
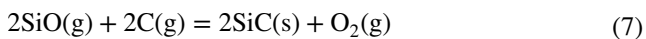


Fig. 14 High-speed camera images of plume propagation from the start of laser irradiation to 4.5 ms after the irradiation starts under defocused distance of **a** 0, **b** 15, **c** 20, **d** 24, and **e** 28 mm

namely the Si grinding sludge and graphite powder. Hence, the surfaces are considered to be naturally oxidized, and the following reactions may happen [10]:



When reactions (7) and (8) are repeated, nanowires are produced from the Si and C gases, as shown in Fig. 19b. In VS and self-catalytic VLS production methods, a continuous supply of raw material from the gas phase [41] and sufficient time for growth are essential for nanowire production.

Figure 20 shows a schematic of the defocusing-induced change in plume shapes, which is the cause of the transition of nanomaterial type from nanoparticles to nanowires. The hypothesized mechanism in Fig. 20 generally agreed with the phenomenon observed in Figs. 15 and 16. Under the

on-focus condition, the plume moved in a single direction (Fig. 20a); thus, a few collisions occurred among the atom clusters and nanodroplets. By contrast, under the defocused conditions, the source material was supplied from various directions due to the swirling movement, resulting in intense collisions of atom clusters and nanodroplets in the plume (Fig. 20b).

The velocity of the plume movement slowed down when the laser was defocused, suggesting that the hot plume travels a short distance through the ambient gas at room temperature, and cooling occurs slowly. Fast cooling and material feeding from only one direction could immediately transform nanodroplets into nanoparticles. By contrast, slow cooling and multidirectional material feeding could saturate the nanodroplets and allow sufficient time for the growth of nanowires or the formation of solid-phase nanowires from the gas phase. In addition to laser irradiation, another well-known method for producing SiC nanowires is to use a furnace kept at around 1400–1600 °C [43, 44]. SiC nanowires grow long when a high temperature is maintained for a long period of time. Under the defocusing condition, the nanowires were considered to have grown because the time

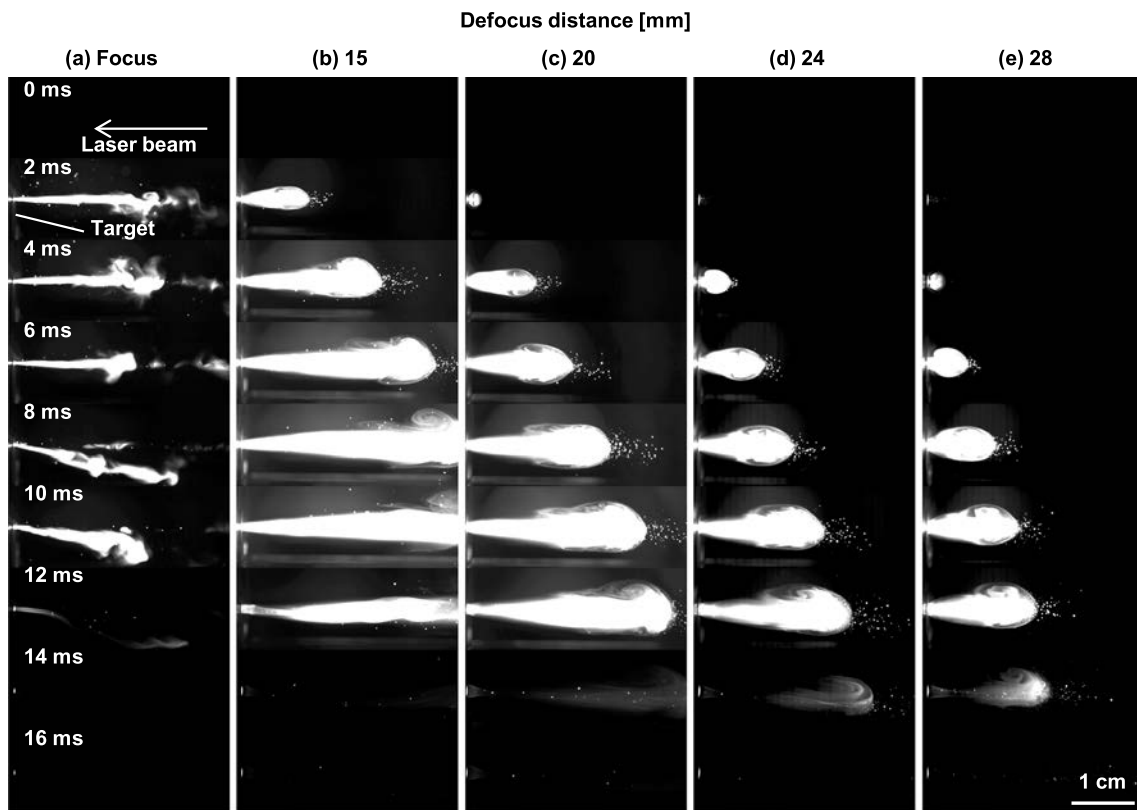


Fig. 15 High-speed camera images of plume propagation from the start of laser irradiation to the end of the irradiation under defocused distance of **a** 0 mm, **b** 15 mm, **c** 20 mm, **d** 24 mm, and **e** 28 mm

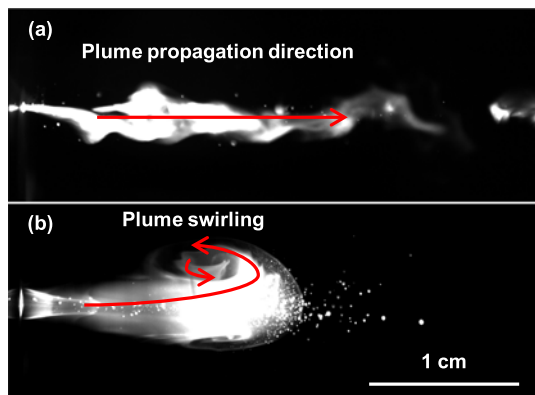


Fig. 16 Enlarged view of the plume under defocus distance of **a** 0 and **b** 28 mm

during which this temperature range could be maintained was longer than that under the on-focusing condition. Previous studies have also shown that nanowires further grow when the pressure is increased from 13 to 101 kPa [19]. The formation of nanowires in this study indicated that the pressure inside the plume was expected to be increased to a

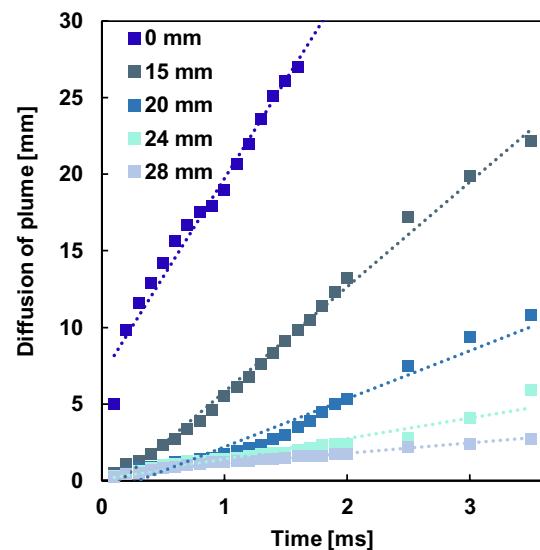


Fig. 17 Differences in plume diffusion distance per unit time due to laser defocusing

similar or higher level compared with that during nanoparticle formation.

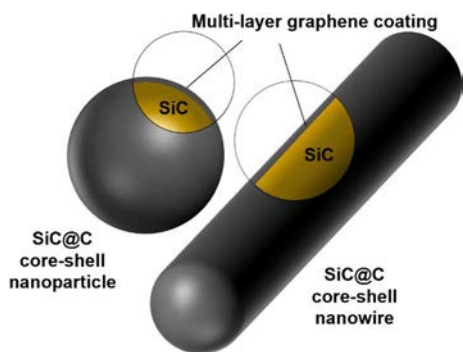


Fig. 18 Schematic of Graphene-coated silicon carbide (SiC@C core-shell) nanoparticles and nanowires

Regarding the mechanism of graphene-layer formation on the surfaces of nanoparticles and nanowires, the layers were coated after the SiC nanoparticles and nanowires were formed. The larger amount of graphite powder in the starting material than Si enabled carbon species to be present in the plume. As a result, a surplus of carbon species was available after the formation of SiC. C plumes have a longer residence time than Si plumes, and this time difference is suitable for C coating [22]. Graphene-layer formation on SiC substrates has also been investigated [45–47], and SiC is considered to have properties that facilitate the deposition of graphene layers on its surface.

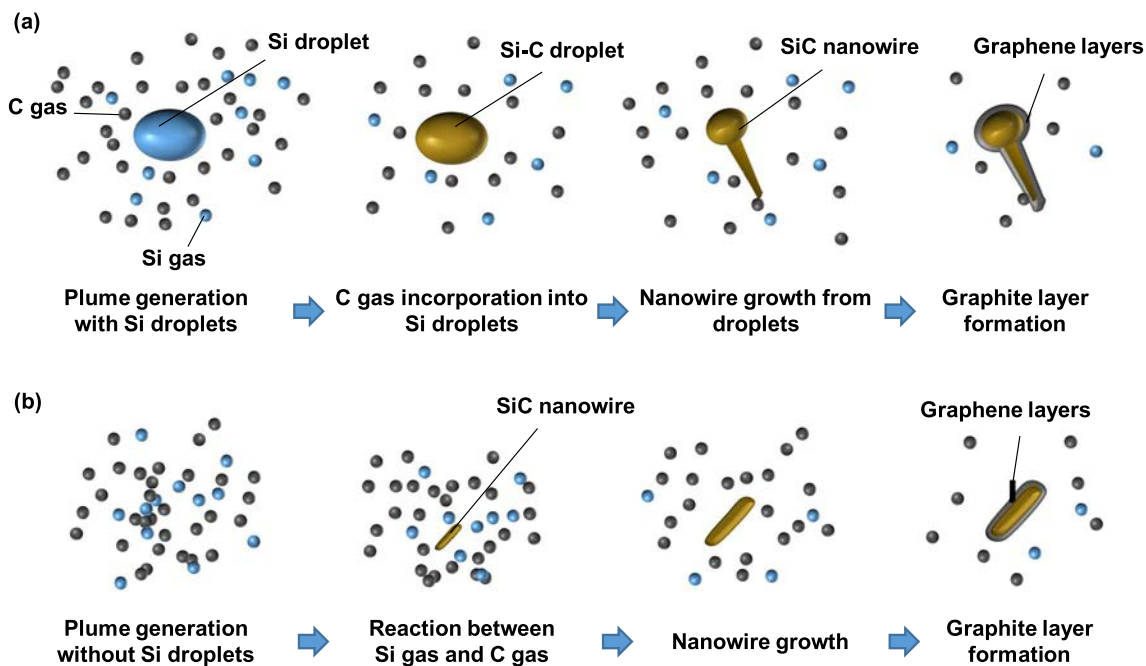


Fig. 19 Schematic of the hypothesized mechanism of SiC nanowire formation: **a** vapor–liquid–solid growth; **b** noncatalyst vapor–solid growth

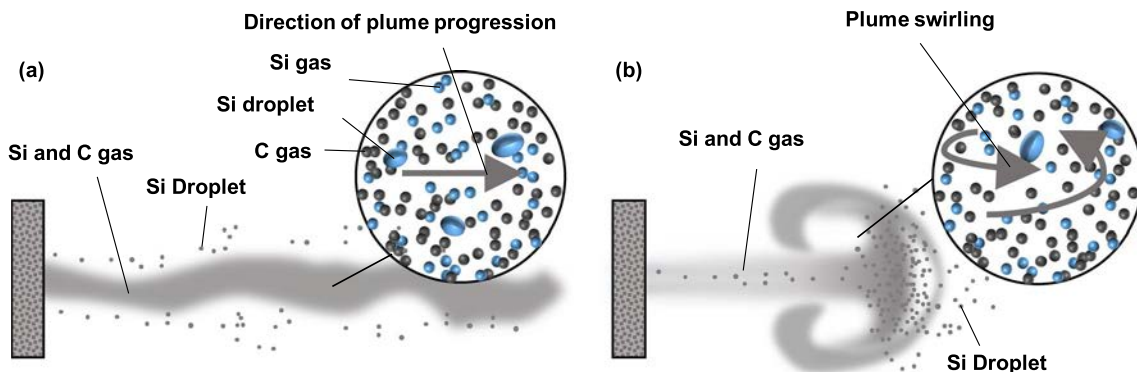


Fig. 20 Schematic of the plume structure under **a** on-focus condition and **b** defocused condition

4 Conclusions

Multilayer graphene-coated SiC nanowires were successfully produced through the laser irradiation of a mixed target of Si grinding sludge and graphite powder by using a suitable defocus distance. Conclusions are presented below.

1. The produced nanostructures are changed from nanoparticles to nanowires by shifting the target position and defocusing the laser beam.
2. The produced nanoparticles and nanowires have a core-shell structure covered by graphene layers, namely SiC@C core-shell nanoparticles and nanowires.
3. The nanowire growth involves two possible mechanisms: VLS and VS, resulting in nanowires with/without tip caps, respectively.
4. The plume generated under on-focus conditions propagates in a single direction at high speed, and that generated under defocus conditions swirls as a vortex moving at a low speed. Under such conditions, the slow cooling speed and multidirectional material supply promote nanowire growth.
5. The graphene layers are deposited by C gas diffusion after the SiC nanostructures are formed.

The produced nanoparticles and nanowires are expected to be used as anode materials for lithium-ion batteries. Nanowires are preferable because of their high strength and flexibility with respect to anode deformation. Nanowires are further expected to be used as materials for bioelectrodes and field emission displays. In this study, the nanowires were grown under noncatalytic conditions. Even for nanowires with chips, the chip part is already capable of self-catalysis without introducing another catalytic material, such as metal. Therefore, they can be used in a wide range of applications where metal contamination causes problems. The quantitative measurement of productivity is important when considering the industrial applicability of the proposed method. We will focus on this topic in our future work.

The results of this research broaden the reuse application of waste Si sludge and demonstrate the possibility of generating new Si/C composite nanomaterials with unique core-shell structures and compositing nanomaterials with other materials. The creation of these new materials from industrial waste is expected to contribute to sustainable manufacturing and industrial symbiosis for the realization of SDGs.

Supplementary Information The online version contains supplementary material available at <https://doi.org/10.1007/s41871-023-00203-8>.

Acknowledgements The authors would like to thank Prof. Yoshiyuki Hattori of Shinshu University, Dr. Kunimitsu Takahashi and Mr.

Akihito Kawai of DISCO Corporation for their valuable suggestions and technical supports. This work was supported by the Japan Society for the Promotion of Science, Grant-in-Aid for Exploratory Research (project number 21K18681).

Author Contributions All authors contributed to the experimental work and data analysis. All authors read and approved the final manuscript.

Funding This study was funded by Japan Society for the Promotion of Science, Grant-in-Aid for Exploratory Research (Project Number 21K18681).

Availability of Data and Materials The authors declare that all data supporting the findings of this study are available within the article.

Declarations

Conflict of interests Jiwang Yan is an editorial board member for “Nanomanufacturing and Metrology” and was not involved in the editorial review, or the decision to publish this article. All authors declare that there are no competing interests.

Open Access This article is licensed under a Creative Commons Attribution 4.0 International License, which permits use, sharing, adaptation, distribution and reproduction in any medium or format, as long as you give appropriate credit to the original author(s) and the source, provide a link to the Creative Commons licence, and indicate if changes were made. The images or other third party material in this article are included in the article's Creative Commons licence, unless indicated otherwise in a credit line to the material. If material is not included in the article's Creative Commons licence and your intended use is not permitted by statutory regulation or exceeds the permitted use, you will need to obtain permission directly from the copyright holder. To view a copy of this licence, visit <http://creativecommons.org/licenses/by/4.0/>.

References

1. Sarti D, Einhaus R (2002) Silicon feedstock for the multi-crystalline photovoltaic industry. *Sol Energy Mater Sol Cells* 72:27–40. [https://doi.org/10.1016/S0927-0248\(01\)00147-7](https://doi.org/10.1016/S0927-0248(01)00147-7)
2. Drouiche N, Cuellar P, Kerker F, Medjahed S, Boutouchent-Guerfi N, Ould Hamou M (2014) Recovery of solar grade silicon from kerf loss slurry waste. *Renew Sustain Energy Rev* 32:936–943. <https://doi.org/10.1016/j.rser.2014.01.059>
3. Hsu HP, Huang WP, Yang CF, Lan CW (2014) Silicon recovery from cutting slurry by phase transfer separation. *Sep Purif Technol* 133:1–7. <https://doi.org/10.1016/j.seppur.2014.06.037>
4. Wang TY, Lin YC, Tai CY, Sivakumar R, Rai DK, Lan CW (2008) A novel approach for recycling of kerf loss silicon from cutting slurry waste for solar cell applications. *J Cryst Growth* 310:3403–3406. <https://doi.org/10.1016/j.jcrysgro.2008.04.031>
5. Wang TY, Lin YC, Tai CY, Fei CC, Tseng MY, Lan CW (2009) Recovery of silicon from kerf loss slurry waste for photovoltaic applications. *Prog Photovoltaics Res Appl* 17:155–163. <https://doi.org/10.1002/pip>
6. Erk C, Brezesinski T, Sommer H, Schneider R, Janek J (2013) Toward silicon anodes for next-generation lithium ion batteries: a comparative performance study of various polymer binders and silicon nanopowders. *ACS Appl Mater Interfaces* 5:7299–7307. <https://doi.org/10.1021/am401642c>
7. Chan CK, Peng H, Liu G, McIlwrath K, Zhang XF, Huggins RA, Cui Y (2008) High-performance lithium battery anodes using

- silicon nanowires. *Nat Nanotechnol* 3:31–35. <https://doi.org/10.1038/nnano.2007.411>
8. Sri Devi Kumari T, Jayakumar D, Prem Kumar T (2013) Nano silicon carbide: a new lithium-insertion anode material on the horizon. *RSC Adv* 3:15028–15034. <https://doi.org/10.1039/c3ra40798e>
 9. Zhang X, Chen Y, Liu W, Xue W, Li J, Xie Z (2013) Growth of n-type 3C-SiC nanoneedles on carbon fabric: toward extremely flexible field emission devices. *J Mater Chem C* 1:6479–6486. <https://doi.org/10.1039/c3tc31189a>
 10. Yang GZ, Cui H, Sun Y, Gong L, Chen J, Jiang D, Wang CX (2009) Simple catalyst-free method to the synthesis of β -SiC nanowires and their field emission properties. *J Phys Chem C* 113:15969–15973. <https://doi.org/10.1021/jp906167s>
 11. Phan HP, Cheng HH, Dinh T, Wood B, Nguyen TK, Mu F, Kamble H, Vadivelu R, Walker G, Hold L, Iacopi A, Haylock B, Dao DV, Lobino M, Suga T, Nguyen NT (2017) Single-crystalline 3C-SiC anodically bonded onto glass: an excellent platform for high-temperature electronics and bioapplications. *ACS Appl Mater Interfaces* 9:27365–27371. <https://doi.org/10.1021/acsmi.7b06661>
 12. Botsoa J, Lysenko V, Géloën A, Marty O, Bluet JM, Guillot G (2008) Application of 3C-SiC quantum dots for living cell imaging. *Appl Phys Lett* 92:1–4. <https://doi.org/10.1063/1.2919731>
 13. Huang F, Fan S, Li X, Qu X, Tian Y, Zhang X, Zhang Z, Dong X, Cao T (2021) Enhanced dielectric and conductivity properties of carbon-coated SiC nanocomposites in the terahertz frequency range. *Nanotechnology* 32. <https://doi.org/10.1088/1361-6528/abf070>
 14. Zhang M, Li ZJ, Zhao J, Gong L, Meng AL, Liu XL, Fan XY, Qi XL (2015) Amorphous carbon coating for improving the field emission performance of SiC nanowire cores. *J Mater Chem C* 3:658–663. <https://doi.org/10.1039/c4tc01658k>
 15. Yang XK, Zhang FL, Wu WT, Tang Y, Yan J, Liu YL, Amatore C, Huang WH (2021) Quantitative nano-amperometric measurement of intravesicular glutamate content and its sub-quantal release by living neurons. *Angew Chemie - Int Ed* 60:15803–15808. <https://doi.org/10.1002/anie.202100882>
 16. Zhang XW, Qiu QF, Jiang H, Zhang FL, Liu YL, Amatore C, Huang WH (2017) Real-time intracellular measurements of ROS and RNS in living cells with single core-shell nanowire electrodes. *Angew Chemie - Int Ed* 56:12997–13000. <https://doi.org/10.1002/anie.201707187>
 17. Momoki K, Manabe T, Li L, Yan J (2020) Silicon nanoparticle generation and deposition on glass from waste silicon powder by nanosecond pulsed laser irradiation. *Mater Sci Semicond Process* 111:104998. <https://doi.org/10.1016/j.mssp.2020.104998>
 18. Momoki K, Yan J (2020) Nanoparticle generation from various types of silicon materials by nanosecond-pulsed laser irradiation. *Appl Phys Express* 13. <https://doi.org/10.35848/1882-0786/ab6935>
 19. Momoki K, Takahashi K, Kobinata K, Kobayashi Y, Kawai A, Yan J (2020) Generating silicon nanofiber clusters from grinding sludge by millisecond pulsed laser irradiation. *Nanomaterials* 10:7–9. <https://doi.org/10.3390/nano10040812>
 20. Hamad S, Podagatlapalli GK, Vendamani VS, Nageswara Rao SVS, Pathak AP, Tewari SP, Venugopal Rao S (2014) Femtosecond ablation of silicon in acetone: tunable photoluminescence from generated nanoparticles and fabrication of surface nanostructures. *J Phys Chem C* 118:7139–7151. <https://doi.org/10.1021/jp501152x>
 21. Švrček V, Sasaki T, Shimizu Y, Koshizaki N (2006) Blue luminescent silicon nanocrystals prepared by ns pulsed laser ablation in water. *Appl Phys Lett* 89:1–3. <https://doi.org/10.1063/1.2397014>
 22. Minami K, Kobinata K, Yan J (2022) Generation of Si@C/SiC@C core-shell nanoparticles by laser irradiation of silicon grinding waste. *Nano Sel* 1–9. <https://doi.org/10.1002/nano.202200001>
 23. Shi W, Zheng Y, Peng H, Wang N, Lee CS, Lee S-T (2000) Laser ablation synthesis and optical characterization of silicon carbide nanowires. *J Am Ceram Soc* 83:3228–3230. <https://doi.org/10.1111/j.1151-2916.2000.tb01714.x>
 24. Gornushkin IB, Panne U (2010) Radiative models of laser-induced plasma and pump-probe diagnostics relevant to laser-induced breakdown spectroscopy. *Spectrochim Acta - Part B At Spectrosc* 65:345–359. <https://doi.org/10.1016/j.sab.2010.03.021>
 25. Kawamura T (1965) Silicon carbide crystals grown in nitrogen atmosphere. *Mineral J* 4:333–355
 26. Hannam AL, Shaffer PTB (1969) Revised X-ray diffraction line intensities for silicon carbide polytypes. *J Appl Crystallogr* 2:45–48. <https://doi.org/10.1107/S0021889869006510>
 27. Capitani GC, Pierro S Di, Tempesta G (2007) The 6H-SiC structure model: further refinement from SCXRD data from a terrestrial moissanite. *Am Mineral* 92:403–407. <https://doi.org/10.2138/am.2007.2346>
 28. Trucano P, Chen R (1975) Structure of graphite by neutron diffraction. *Nature* 258:136–137. <https://doi.org/10.1038/258136a0>
 29. Okada Y, Tokumaru Y (1984) Precise determination of lattice parameter and thermal expansion coefficient of silicon between 300 and 1500 K. *J Appl Phys* 56:314–320. <https://doi.org/10.1063/1.333965>
 30. Zhang Y, Shen Z, Ni X (2014) Modeling and simulation on long pulse laser drilling processing. *Int J Heat Mass Transf* 73:429–437. <https://doi.org/10.1016/j.ijheatmasstransfer.2014.02.037>
 31. Milán M, Laserna JJ (2001) Diagnostics of silicon plasmas produced by visible nanosecond laser ablation. *Spectrochim Acta - Part B At Spectrosc* 56:275–288. [https://doi.org/10.1016/S0584-8547\(01\)00158-6](https://doi.org/10.1016/S0584-8547(01)00158-6)
 32. Zhang S, Wang Q, Lin T, Zhang P, He P, Paik KW (2021) Cu–Cu joining using citrate coated ultra-small nano-silver pastes. *J Manuf Process* 62:546–554. <https://doi.org/10.1016/j.jmapro.2020.11.043>
 33. Liu L, Shi R, Zhang S, Liu W, Huang S, Chen Z (2023) Effects of Ag shell on electrical, thermal and mechanical properties of Cu@Ag composite solder preforms by electromagnetic compaction for power electronics. *Mater Charact* 197:112702. <https://doi.org/10.1016/j.matchar.2023.112702>
 34. Morales AM, Lieber CM (1998) A laser ablation method for the synthesis of crystalline semiconductor nanowires. *Science* (80-) 279:208–211. <https://doi.org/10.1126/science.279.5348.208>
 35. Lee JS, Byeun YK, Lee SH, Choi SC (2008) In situ growth of SiC nanowires by carbothermal reduction using a mixture of low-purity SiO₂ and carbon. *J Alloys Compd* 456:257–263. <https://doi.org/10.1016/j.jallcom.2007.02.010>
 36. Liu G, Su G, Wang W, Wang F, Wei H, Dang L (2022) A novel method for preparation of SiC/SiO₂ nanocables and photoluminescence performance study. *Appl Phys A Mater Sci Process* 128:1–9. <https://doi.org/10.1007/s00339-021-05209-x>
 37. Kokai F, Inoue S, Hidaka H, Uchiyama K, Takahashi Y, Koshio A (2013) Catalyst-free growth of amorphous silicon nanowires by laser ablation. *Appl Phys A Mater Sci Process* 112:1–7. <https://doi.org/10.1007/s00339-012-7169-y>
 38. Lv KM, Yang J, Niu KY, Wang HL, Sun J, Du XW (2009) Synthesis of Si-C nanostructures by laser ablation of silicon target in n-heptane vapor. *Mater Lett* 63:2492–2494. <https://doi.org/10.1016/j.matlet.2009.08.049>
 39. Kokai F, Uchiyama K, Shimazu T, Koshio A (2010) Fabrication of two types of one-dimensional Si-C nanostructures by laser ablation. *Appl Phys A Mater Sci Process* 101:497–502. <https://doi.org/10.1007/s00339-010-5886-7>

40. Wei J, Li K, Chen J, Yuan H (2011) Synthesis of centimeter-scale ultra-long SiC nanowires by simple catalyst-free chemical vapor deposition. *J Cryst Growth* 335:160–164. <https://doi.org/10.1016/j.jcrysgro.2011.09.021>
41. Huang H, Fox JT, Cannon FS, Komarneni S (2011) In situ growth of silicon carbide nanowires from anthracite surfaces. *Ceram Int* 37:1063–1072. <https://doi.org/10.1016/j.ceramint.2010.11.022>
42. Cetinkaya S, Eroglu S (2011) Chemical vapor deposition of C on SiO₂ and subsequent carbothermal reduction for the synthesis of nanocrystalline SiC particles/whiskers. *Int J Refract Met Hard Mater* 29:566–572. <https://doi.org/10.1016/j.ijrmhm.2011.03.005>
43. Kao K, Jiang M, Ding L, Lin W, Chen J (2019) Catalytic synthesis of SiC nanowires in an open system. *J Am Ceram Soc* 102:3070–3075. <https://doi.org/10.1111/jace.16299>
44. Hu L, Zou Y, Li CH, Liu JA, Shi YS (2020) Preparation of SiC nanowires on graphite paper with silicon powder. *Mater Lett* 269:127444. <https://doi.org/10.1016/j.matlet.2020.127444>
45. Emtsev KV, Bostwick A, Horn K, Jobst J, Kellogg GL, Ley L, McChesney JL, Ohta T, Reshanov SA, Röhl J, Rotenberg E, Schmid AK, Waldmann D, Weber HB, Seyller T (2009) Towards wafer-size graphene layers by atmospheric pressure graphitization of silicon carbide. *Nat Mater* 8:203–207. <https://doi.org/10.1038/nmat2382>
46. Yazdi GR, Vasiliauskas R, Iakimov T, Zakharov A, Syväjärvi M, Yakimova R (2013) Growth of large area monolayer graphene on 3C-SiC and a comparison with other SiC polytypes. *Carbon N Y* 57:477–484. <https://doi.org/10.1016/j.carbon.2013.02.022>
47. Strupinski W, Grodecki K, Wyszomolek A, Stepniewski R, Szkopek T, Gaskell PE, Grüneis A, Haberer D, Bozek R, Krupka J, Baranowski JM (2011) Graphene epitaxy by chemical vapor deposition on SiC. *Nano Lett* 11:1786–1791. <https://doi.org/10.1021/nl200390e>



Kyosuke Kobinata received his Ph.D. from Chiba University, Japan, in 2014 and currently works for DISCO Corporation. His research interests include semiconductor manufacturing and silicon sludge recycling.



Jiwang Yan received his Ph.D. from Tohoku University, Japan, in 2000 and is currently a professor of Mechanical Engineering at Keio University (2012–now), leading the Laboratory for Precision Machining and Nano-Processing. His research areas include ultraprecision machining, micro/nano-manufacturing, laser processing, nanomaterials, and nanomechanics.

Publisher's Note Springer Nature remains neutral with regard to jurisdictional claims in published maps and institutional affiliations.



Kanon Minami received her Bachelor's degree and Master's degree in Mechanical Engineering from Keio University in 2021 and 2023, respectively. She is currently a Ph.D. student in Mechanical Engineering at Keio University under supervision of Prof. Jiwang Yan. Her research interests include laser processing and micro-/nano-manufacturing.